JOURNAL OF COMPUTATIONAL PHYSICS 106, 115–124 (1993)

Application of Vorticity Integral Conditioning to Chebyshev Pseudospectral Formulation for the Navier–Stokes Equations

HOA D. NGUYEN AND SEUNGHO PAIK

Idaho National Engineering Laboratory EG & G Idaho, Inc., Idaho Falls, Idaho 83415

AND

JACOB N. CHUNG

Department of Mechanical and Materials Engineering, Washington State University, Pullman, Washington 99164

Received April 26, 1991

A pseudospectral method based on the vorticity-stream function formulation is proposed for the solution of two-dimensional, time-dependent flow of an incompressible fluid. It features the high resolution and computational economy of Chebyshev collocation and the combined second-order Adams–Bashforth and Crank–Nicolson time integration schemes. Precise treatment for the vorticity condition is accomplished by the use of conditions of integral type. Numerical experiments indicate that the pseudospectral method is capable of producing results comparable to those obtained by finite differences with fewer unknowns and is superior in accuracy for the same number of nodal points.

1. INTRODUCTION

Predicting two-dimensional flow fields of an incompressible fluid requires the simulataneous solution of the continuity and momentum equations with pressure and velocity components employed as dependent variables. However, this treatment, known as the primitive variables approach, suffers the disadvantage that the coupled solution method leads to exceedingly large numerical computations. Moreover, difficulties are also encountered due to the absence of boundary conditions for the pressure. In the alternative approach based on the vorticity and stream function as dependent variables, vector identities are used to eliminate the pressure from the aforementioned set of governing equations. In this manner, the number of equations is reduced by one and the complications brought about by the coupled nature of the equations for incompressible flows is removed. Although the latter approach has been and is very often preferred, a difficulty still remains in that the specification of the boundary condition for the vorticity is troublesome since the no-slip condition at a solid boundary cannot be translated into equivalent conditions of boundary-value type for the vorticity. Among the techniques proposed so far to circumvent such a difficulty, the influence matrix method and the vorticity integral conditions are considered most appropriate in the sense that they rely on a rigorous mathematical foundation and carry a physical interpretation.

Regardless of the differences between these two methods, both necessitates a set of auxiliary functions, to be discussed later in the paper, for decomposing the vorticity field. According to our literature survey, the two methods have been adapted to finite differences [1] and finite elements [2, 3] in the solution of a number of flow problems. In another branch of numerical methodology, i.e., spectral methods, a study has been conducted to address the issue of the applicability of the concepts in conjunction with Chebyshev approximations [4]. However, this study is limited to flows within geometrically simple boundaries, such as flows around cylindrical or spherical bodies. A more recent account concerning this subject has been the work of Chaouche an his co-workers [5], where they combined a pseudospectral scheme with the influence matrix technique to investigate the transport of heat and momentum driven by buoyancy and rotation in an annular domain. To the best of our knowledge, no one has ever attempted to study the effectiveness of a direct use of the vorticity integral conditions for solving the Navier–Stokes equations by means of spectral methods for problems with two nonperiodic directions. Such assessment is worthwhile because the vorticity integral conditions could be an alternative option besides the influence matrix method, particularly in view of the fact that they bear a unique physical meaning with respect to the conservation of the total vorticity [1]. Thus, the objective

0021-9991/93 $5.00

of this research is two fold. One is to establish a spectral framework suitable for the implementation of the vorticity integral constraints which are a direct consequence of the Green's theorem, and the other is to demonstrate the adequacy of the procedure in nonperiodic two-dimensional flows. In particular, we shall extend the Chebyshev expansion model of Ku and Hatziavramidis [6] to time-dependent flows, taking into account the mathematically sound vorticity constraints. In fact, as pointed out in [1], any approximation to the vorticity boundary value could lead to local as well as global discrepancies even for comparable calculations.

2. MATHEMATICAL FORMULATION

2.1. *Governing Equations*

For the two-dimensional motion of an isothermal and incompressible Newtonian fluid, the flow field at any time may be calculated by simultaneously solving for the variables' vorticity and stream function. These unknowns are governed by the following system of equations:

$$\frac{\partial \zeta}{\partial t} + \mathbf{u} \cdot \nabla \zeta = \frac{1}{\mathrm{Re}} \nabla^2 \zeta \qquad \text{in } \Omega, \tag{1}$$

$$\nabla^2 \psi = \zeta \qquad \text{in } \Omega. \tag{2}$$

In the vorticity transport equation (1), the time rate of change of vorticity is influenced by convection and diffusion mechanisms whereas the elliptic equation (2) determines the instantaneous stream function in terms of the vorticity field. In the above equations, Re is the Reynolds number based on a characteristic length and a characteristic velocity of the flow, t is the dimensionless time, $\mathbf{u}$ is the dimensionless velocity vector, ζ and ψ are the dependent variables representing the vorticity and the stream function, respectively. The velocity is calculated from the relationship

$$\mathbf{u} = \mathbf{i} \frac{\partial \psi}{\partial y} - \mathbf{j} \frac{\partial \psi}{\partial x}, \tag{3}$$

where $\mathbf{i}$ and $\mathbf{j}$ are the unit vectors in the x and y directions, respectively. In order to obtain a specific solution to the above set of equations, we need to prescribe initial and boundary conditions consistent with the physical nature of the flow. Generally, these conditions are obtained from the fact that viscosity causes the flowing fluid to adhere to the solid surface. This condition, when imposed in the stream function and vorticity formulation, leads to the two following boundary conditions:

$$\psi|_{\partial\Omega} = \psi_0 \qquad \text{and} \qquad \left.\frac{\partial \psi}{\partial \mathbf{n}}\right|_{\partial\Omega} = \mathbf{u}_\tau, \tag{4}$$

where we have denoted the normal vector as $\mathbf{n}$, the boundary of the flow domain as $\partial\Omega$, the relative tangential velocity as $\mathbf{u}_\tau$ which can, for generality, be a function of time, and the boundary value of the stream function as ψ_0. In particular, if the normal velocity on the boundary is zero, ψ_0 is an arbitrary constant and, for simplicity, will be set to zero hereafter. As far as generality is concerned, both $\mathbf{u}_\tau$ and ψ_0 may depend on time as well as space.

Regarding the initial condition, the stream function and vorticity are taken to be zero,

$$\psi(0, \mathbf{r}) = 0 \qquad \text{and} \qquad \zeta(0, \mathbf{r}) = 0 \qquad \text{in } \Omega, \tag{5}$$

where $\mathbf{r}$ is the position vector. This condition corresponds to the situation that the fluid is initially at rest.

2.2. *Vorticity Integral Conditions*

The presence of the no-slip condition, together with the fact that the boundary of a two-dimensional solid must form a streamline, creates an unusual difficulty. This is mainly due to the overspecification of the boundary conditions for the stream function, whereas no condition for the vorticity is available. However, the two methods mentioned in the introduction lead to a way to impose conditions on the vorticity in terms of the boundary values of the stream function and of its normal derivative. Due to its iterative character, the procedure proposed by MacKinnon *et al.* [3], the method is not well suited to transient problems; therefore, we shall follow the method proposed by Quartapelle [1]. The theory behind the derivation of the vorticity integral conditions is nothing more than an application of the well-known Green's identity [7, 8],

$$\int_\Omega (\phi \nabla^2 \psi - \psi \nabla^2 \phi)\, dA = \int_{\partial\Omega} \left(\phi \frac{\partial \psi}{\partial \mathbf{n}} - \psi \frac{\partial \phi}{\partial \mathbf{n}} \right) dS. \tag{6}$$

The vorticity conditions can be obtained by choosing ϕ in (6) to be a function η that satisfies the Laplace equation, i.e., $\nabla^2 \eta = 0$. Thus, for the particular case $\psi_0 = 0$, one obtains the integral conditions,

$$\int_\Omega \zeta \eta\, dA = \int_{\partial\Omega} \mathbf{u}_\tau \eta\, dS. \tag{7}$$

Some physical insight can be gained from the above equation. Of particular importance is the case for $\eta = 1$, under which Eq. (7) may be interpreted as follows: The total vorticity in the system bounded by $\partial\Omega$ depends only on the circulation of the velocity along the periphery of the flow domain. Coming now to a spatially discrete version of the problem, it is immediate to see that there are as many η functions as the number of boundary points [1]. By

following this argument, each η_i satisfies the Laplace equation with a value of zero everywhere along the boundary except at one grid point where the value is one. This statement is equivalent to

$$\nabla^2\eta_i = 0, \qquad \eta_i|_{\partial\Omega} = \delta_{ij}, \tag{8}$$

for $i, j = 1, 2, ..., NS$, where NS denotes the total number of nodal points located on the boundary. Note that δ_{ij} is the usual notation representing the Kronecker delta.

3. METHOD OF SOLUTION

In the past, numerous versions of spectral methods have been constructed in the form suitable for the calculations to be carried out in either spectral space, physical space, or both by means of FFT (fast Fourier transform, of which Chebyshev is a special case) [9, 10]. Particularly attractive for the present work is the formulation due to Ku and Hatziavramidis [6] who, in the context of Chebyshev collocation, devised a matrix multiplication technique capable of calculating the first and second derivatives of a function in physical space. While such calculation using the direct method requires N^2 multiplications, the same can be achieved in $N\log_2(N)$ operations by FFT. Depending on the computer, the matrix multiplication method is more efficient for small N with the crossover point being somewhere between 16 and 64 which is sufficient to provide adequate resolution to the test problems to be considered in the next section. Based on this consideration, they introduced a new spectral model which does not require the FFT.

3.1. *Chebyshev Expansion*

As a first step toward our ultimate goal, we shall review the methodology of evaluating derivatives of a function, say $f(x)$, with $x \in [-1, 1]$. The value of the function at the Gauss–Lobatto points $\{x_i,\ i = 0, 1, 2, ..., N\}$, defined as $\cos(i\pi/N)$, are given by

$$f_i = f(x_i) = \sum_{j=0}^{N} a_j T_j(x_i), \tag{9}$$

where T_j is the Chebyshev polynomial of order j. In matrix notation, it becomes

$$\mathbf{f} = \mathbf{T}\mathbf{a}. \tag{10}$$

For convenience, both matrix and series notations will be used interchangeably throughout. Provided f is differentiable, the first derivative of f at the collocation points can be computed numerically from the expression:

$$\mathbf{f}' = \mathbf{T}\mathbf{a}^{(1)}, \tag{11}$$

where a superscript (1) has been used to denote first derivative coefficients. The matrix $\mathbf{T}$ in Eqs. (10) and (11) is the $(N+1)\times(N+1)$ square matrix with the following entries

$$T_{ij} = T_j(x_i). \tag{12}$$

By taking advantage of the recursion formulas concerning derivative of Chebyshev polynomials as given in most standard texts on special functions, it is possible to deduce the following relationship:

$$\mathbf{a}^{(1)} = \mathbf{G}^{(1)}\mathbf{a}, \tag{13}$$

where $\mathbf{G}^{(1)}$ is by definition the first derivative matrix. The components of $\mathbf{G}^{(1)}$ can be shown to be

$$G_{ij}^{(1)} = \begin{cases} 0, & i \geqslant j \text{ or } i+j \text{ even} \\ 2(j-1)/C_i, & \text{otherwise} \end{cases} \tag{14}$$

and the constant C_i takes on the value of two if i equals zero and one otherwise. Since $\mathbf{T}$ is nonsingular, its inverse exists and so does the inverse Chebyshev transform. This property allows us to rewrite Eq. (11) in a form free of spectral coefficients, i.e.,

$$\begin{aligned} \mathbf{f}' &= \mathbf{T}\mathbf{G}^{(1)}\hat{\mathbf{T}}\mathbf{f} \\ &= \hat{\mathbf{G}}^{(1)}\mathbf{f}, \end{aligned} \tag{15}$$

where a hat is used to indicate the inverse transform of the corresponding operation. In a similar fashion, the equation for the second derivative can also be derived to give

$$\begin{aligned} \mathbf{f}'' &= \mathbf{T}\mathbf{G}^{(1)}\mathbf{G}^{(1)}\hat{\mathbf{T}}\mathbf{f} \\ &= \hat{\mathbf{G}}^{(2)}\mathbf{f}. \end{aligned} \tag{16}$$

For completeness, the ith row and the jth column entry of the inverse transform of $\mathbf{T}$ may be given in closed form as

$$\hat{T}_{ij} = \frac{1}{NC_iC_j} T_i(x_j), \tag{17}$$

whereas values at other locations can be obtained accordingly. It is worthwhile to note that the steps leading to Eq. (17) primarily involve the utilization of the orthogonality properties of Chebyshev polynomials. It is now apparent that the derivatives of a function obeying the differentiality criteria can be computed accurately and efficiently without the need of a fast transform.

3.2. *Spectral Representation of the Flow Equations*

As one may recognize, the task of converting the vorticity transport equation and the stream function equation to

spectral form is now trivial. Indeed, by substituting appropriate spectral expressions for the derivatives, the governing equations can be rewritten as

$$\frac{d\zeta_{i,k}}{dt}+N_{i,k}=\frac{1}{\mathrm{Re}}\left[\sum_{i'=0}^{NX} G\hat{X}^{(2)}_{ii'}\zeta_{i',k}+\sum_{k'=0}^{NY} G\hat{Y}^{(2)}_{kk'}\zeta_{i,k'}\right], \quad (18)$$

$$\sum_{i'=0}^{NX} G\hat{X}^{(2)}_{ii'}\psi_{i',k}+\sum_{k'=0}^{NY} G\hat{Y}^{(2)}_{kk'}\psi_{i,k'}=\zeta_{i,k}, \quad (19)$$

in which $(NX+1)$ and $(NY+1)$ are the numbers of collocation points in the x and y directions, respectively. Note that $\zeta_{i,k}$ and $\psi_{i,k}$ are physically meaningful quantities, not spectral coefficients, associated with the point (x_i, y_k). For ease of simplifying the notation, the spectral expression of the convection term has been abbreviated as $N_{i,k}$. Explicitly, it represents

$$N_{i,k}\equiv\left[\sum_{k'=0}^{NY} G\hat{Y}^{(1)}_{kk'}\psi_{i,k'}\right]\left[\sum_{i'=0}^{NX} G\hat{X}^{(1)}_{ii'}\zeta_{i',k}\right]-\left[\sum_{i'=0}^{NX} G\hat{X}^{(1)}_{ii'}\psi_{i',k}\right]\left[\sum_{k'=0}^{NY} G\hat{Y}^{(1)}_{kk'}\zeta_{i,k'}\right], \quad (20)$$

where $\mathbf{G\hat{X}}$ and $\mathbf{G\hat{Y}}$ are the derivative matrices with respect to x and y, respectively. They are defined exactly the same way as $\hat{G}$ and are, in fact, identical if $NX=NY$.

3.3. *Time Discretization*

Perhaps, one of the most popular schemes suited for integrating the time evolution equation (18) is the combined algorithms of Adams–Bashforth and Crank–Nicolson. Such combination, when applied properly, would lead to an effective scheme of second-order accuracy. If the nonlinear convection and viscous diffusion terms are treated by the former and the latter respectively, there results two linear systems:

$$\frac{2\mathrm{Re}}{\Delta t}\zeta^{n+1}_{i,k}-\sum_{i'=0}^{NX} G\hat{X}^{(2)}_{ii'}\zeta^{n+1}_{i',k}-\sum_{k'=0}^{NY} G\hat{Y}^{(2)}_{kk'}\zeta^{n+1}_{i,k'}=F^{n}_{i,k}, \quad (21)$$

$$\sum_{i'=0}^{NX} G\hat{X}^{(2)}_{ii'}\psi^{n+1}_{i',k}+\sum_{k'=0}^{NY} G\hat{Y}^{(2)}_{kk'}\psi^{n+1}_{i,k'}=\zeta^{n+1}_{i,k}, \quad (22)$$

where Δt is the time increment and the superscript n indicates the time level. Since this combined scheme is not self-starting, the convection term is treated differently at the first time level and in a fashion that preserves consistent accuracy. The right-hand side of Eq. (21) can be expressed in a compact form as

$$F^{n}_{i,k}=\frac{2\mathrm{Re}}{\Delta t}\zeta^{n}_{i,k}+\sum_{i'=0}^{NX} G\hat{X}^{(2)}_{ii'}\zeta^{n}_{i',k}+\sum_{k'=0}^{NY} G\hat{Y}^{(2)}_{kk'}\zeta^{n}_{i,k'}-2\mathrm{Re}\begin{cases}N^{n+1/2}_{i,k}, & n=0,\\ 1.5N^{n}_{i,k}-0.5N^{n-1}_{i,k}, & n\neq 0.\end{cases} \quad (23)$$

As is indicated in Eq. (23), all the nodal values are readily available from previous time steps; hence the combined time differencing technique treats the nonlinearities in the vorticity transport equation in an explicit manner. It is also worthwhile to point out that the left-hand side of Eqs. (21) and (22) are linear and unchanged with time; thus each can be factored into upper and lower matrices once and for all. After the factorization, only backward and forward substitutions are needed for the solution to advance from one time level to the next.

3.4. *Vorticity Decomposition*

In steady flow, Eqs. (21) and (22) can be solved and the satisfaction of requirement (7) can be reached by an iterative procedure. However, this procedure is not feasible for transient flow problems due to the large number of iterations involved. In view of the theory of linear partial differential equations, we assume the vorticity as a linear combination of a set of auxiliary functions as

$$\zeta=w^0+\sum_{j=1}^{NS} q_j w^j, \quad (24)$$

where $\{q_j, j=1, 2, ..., NS\}$ is a set of decomposition coefficients to be determined in such a way to ensure the vorticity integral conditions be satisfied. Also each member of the set $\{w^j, j=1, 2, ..., NS\}$ is the solution of the Helmholtz equation,

$$\frac{2\mathrm{Re}}{\Delta t}w^{j}_{i,k}-\sum_{i'=0}^{NX} G\hat{X}^{(2)}_{ii'}w^{j}_{i',k}-\sum_{k'=0}^{NY} G\hat{Y}^{(2)}_{kk'}w^{j}_{i,k'}=0, \quad (25)$$

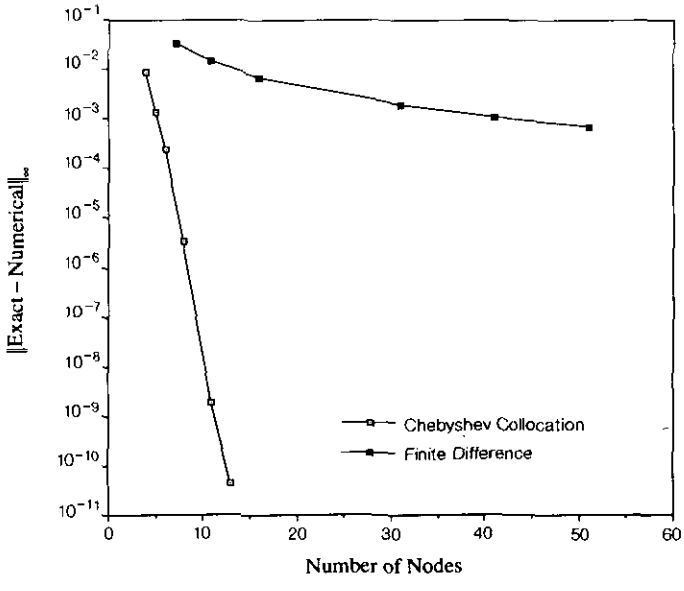

FIG. 1. Convergence rate comparison.

subjected to the Dirichlet boundary conditions,

$$w^j|_{\partial\Omega} = \delta_{jm}, \tag{26}$$

for $j, m = 1, 2, ..., NS$. In contrast to the rest of w^j, the remaining auxiliary function w^0 is the solution of the nonhomogeneous problem (21),

$$\frac{2\mathrm{Re}}{\Delta t} w^0_{i,k} - \sum_{i'=0}^{NX} G\hat{X}^{(2)}_{ii'} w^0_{i',k} - \sum_{k'=0}^{NY} G\hat{Y}^{(2)}_{kk'} w^0_{i,k'} = F^n_{i,k}, \tag{27}$$

in conjunction with homogeneous Dirichlet-type boundary condition,

$$w^0|_{\partial\Omega} = 0. \tag{28}$$

Upon substitution of Eq. (24) into the vorticity integral conditions (7), there results a system of linear algebraic equations,

$$\sum_{j=1}^{NS} q_j \int_\Omega \eta_m w^j \, dA = \int_\Omega \eta_m w^0 \, dA + \int_{\partial\Omega} \mathbf{u}_\tau \eta_m \, dS, \tag{29}$$

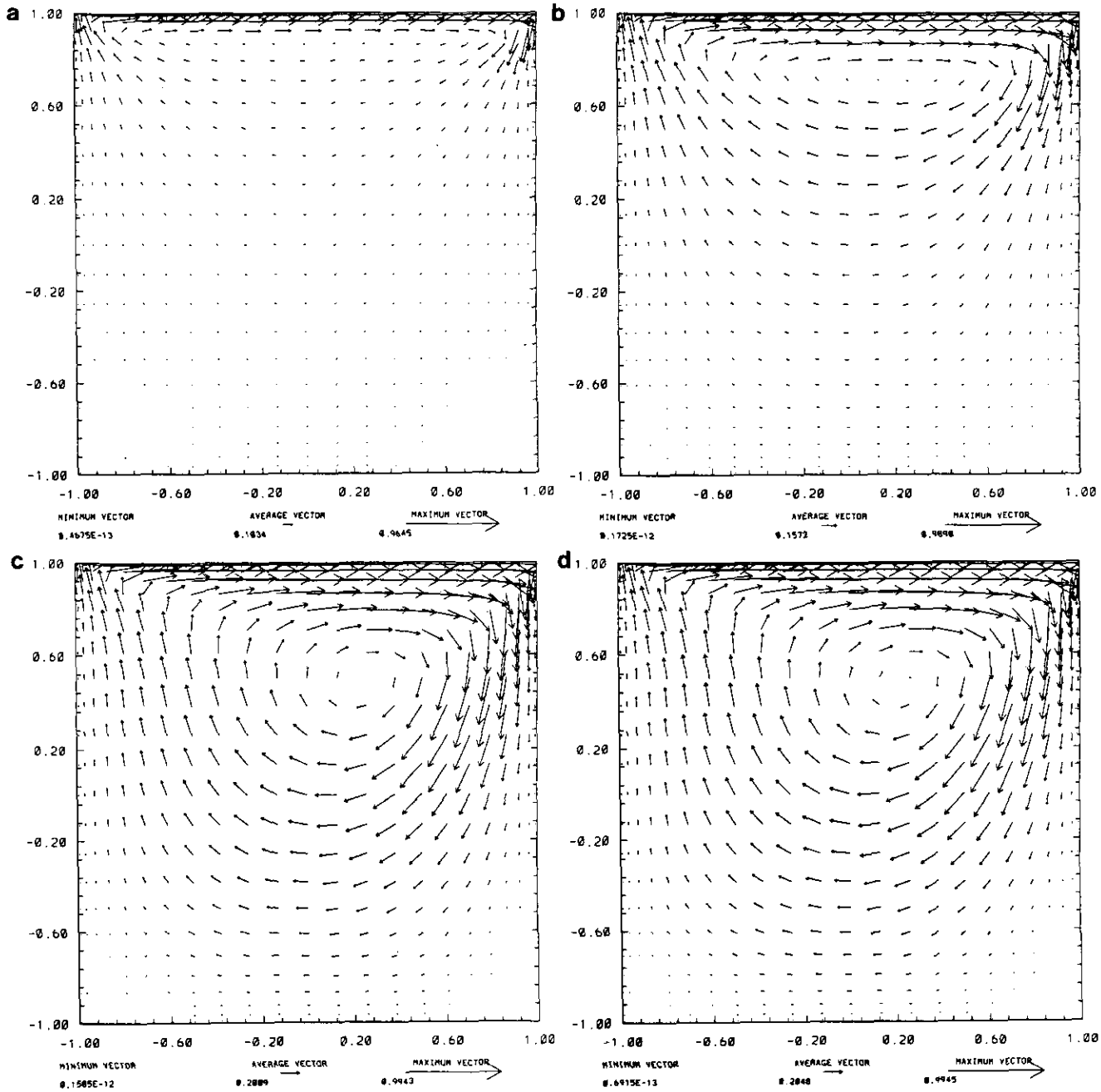

FIG. 2. Velocity vector for Re = 100: (a) $t = 0.1$; (b) $t = 1$; (c) $t = 10$; (d) $t = 40$.

which can easily be solved for q_j's. Inspection of Eq. (29) also reveals that time dependence only occurs in the right-hand side, and therefore the LU factorization of the matrix can be done once and for all at the beginning of the calculation. To end this discussion, it is remarked that the integrals in Eq. (29) are evaluated by the trapezoidal rule in all the calculations to be presented in the subsequent section.

4. RESULTS AND DISCUSSION

Although the main focus of this article is the solution of the Navier–Stokes equations, the application of a mixed time differencing technique has led to a series of Helmholtz and Poisson equations to be solved. Due to the couplings between the stream function and vorticity in the convective terms, numerical assessment is difficult. To simplify our task, it is sufficient to consider the Helmholtz equation, defining on a unit square, i.e., $x, y \in [0, L] \times [[0, L]$ of the form

$$\frac{\partial^2 \Theta}{\partial x^2} + \frac{\partial^2 \Theta}{\partial y^2} + \alpha \Theta = 0, \tag{30}$$

subjected to the boundary conditions: $\Theta(0, y) = \Theta(L, y) = \Theta(x, L) = 0$, and $\Theta(x, 0) = 1$. As can be seen from Eq. (30), Poisson equation is recovered when $\alpha = 0$. The justification for choosing this test problem is the fact that analytical solution is available [11]. Furthermore, it has some features similar to the driven cavity problem we are going to consider in order to assess the capability of the proposed method.

To examine the capability of the Chebyshev expansion method, Eq. (30) is solved for a number of different grids with an equal number of unknowns in both directions by spectral and finite difference methods. Fig. 1 is the result of our convergence study where the maximum norm of the error is plotted against the number of degrees of freedom used. From this figure, the linearity of the spectral curve implies that the truncation error associated with Chebyshev expansion decreases exponentially. On the contrary, the rate of convergence of finite difference method shows little sensitivity with respect to the number of nodal points. These behaviors demonstrate that $\log \|\text{Exact} - \text{Numerical}\|_\infty$ is proportional to N for Chebyshev collocation, and to $\log(N)$ for the traditional finite difference method. Much of the discussion here is also applicable to the finite element method as well, because both finite difference and finite elements exhibit the same type of convergence behavior. With regard to accuracy, the pseudospectral method is superior to the traditional methods; however, such an attractive feature is gained at the expense of a large computing time. This conclusion may be substantiated by the following consideration: For a fixed level of accuracy, say 0.01, the spectral method required five collocation points, whereas the finite difference method needed 20 nodes in each direction, including those at the ends. Provided that the preprocessing work is the same for both methods, which is likely to be the case in many problems, the overall computing expense is essentially the cost of solving a system of equations. For this problem, the size of the matrix to be inverted for the spectral method is 9×9 and it is 324×324 for finite difference, but it should be kept in mind that the latter is banded, whereas the former is full. Depending on the linear system solver that one uses, this information can be directly related to the computational cost. In this particular example, the computing time associated with spectral analysis is likely to be less than the finite difference approximation; however, it increases very rapidly with increasing the number of collocation points. In many problems, transition and turbulent flows, for instance, the success of a numerical scheme may not be entirely measured by the level of intensiveness of the com-

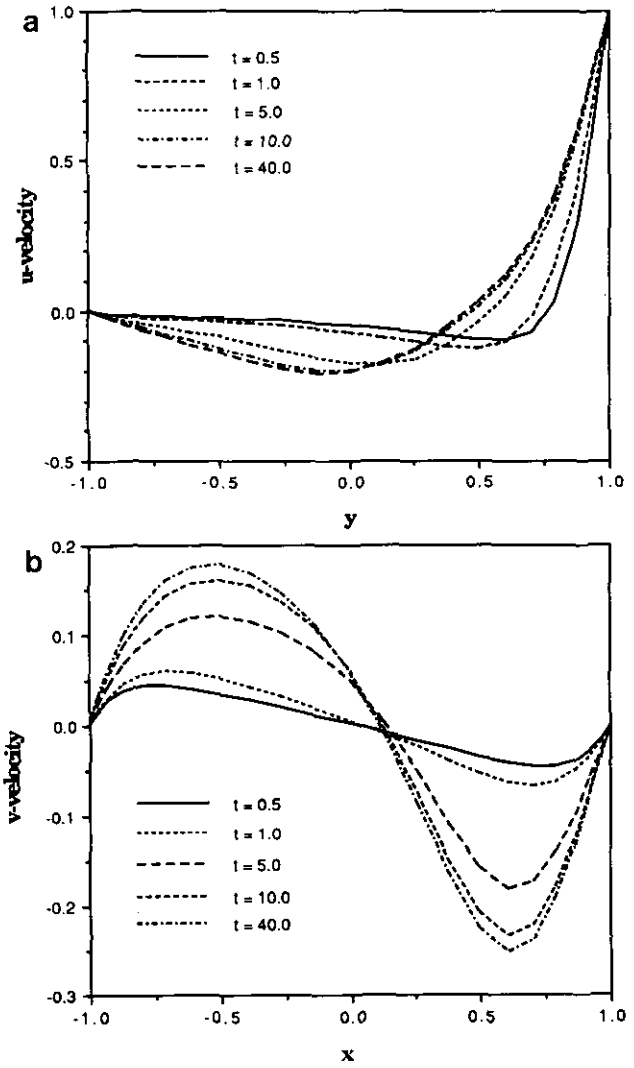

FIG. 3. *Time variation of velocity for Re = 100:* (a) *u*-velocity along *y*-axis; (b) *v*-velocity along *x*-axis.

putation, but by the accuracy and the spatial resolution capability as well. Therefore, the proposed scheme would be useful tool for modeling such flows.

In the remainder of this section, we shall apply our formulation to an internal flow in a square cavity generated by a moving lid. The cavity, centered at the origin of the x-y coordinate system, is bounded by rigid and impermeable side walls of equal length, $2L$, with the upper surface covered by a lid whose motion is constrained in the direction from left to right and parallel to the horizontal x-axis. This problem has been used from time to time for numerical assessment of finite differences [12] and finite elements [13]. In recent years, it has become a popular test case to appraise the spectral schemes [14, 15] because of the singularities in the flow that have significant impact on the numerical properties of the algorithm. As noted by Schultz *et al.* [14], the existence of the corner singularities hurts the exponential convergence character of spectral methods, and therefore the driven cavity flow would serve as a good model problem to evaluate the performance of spectral

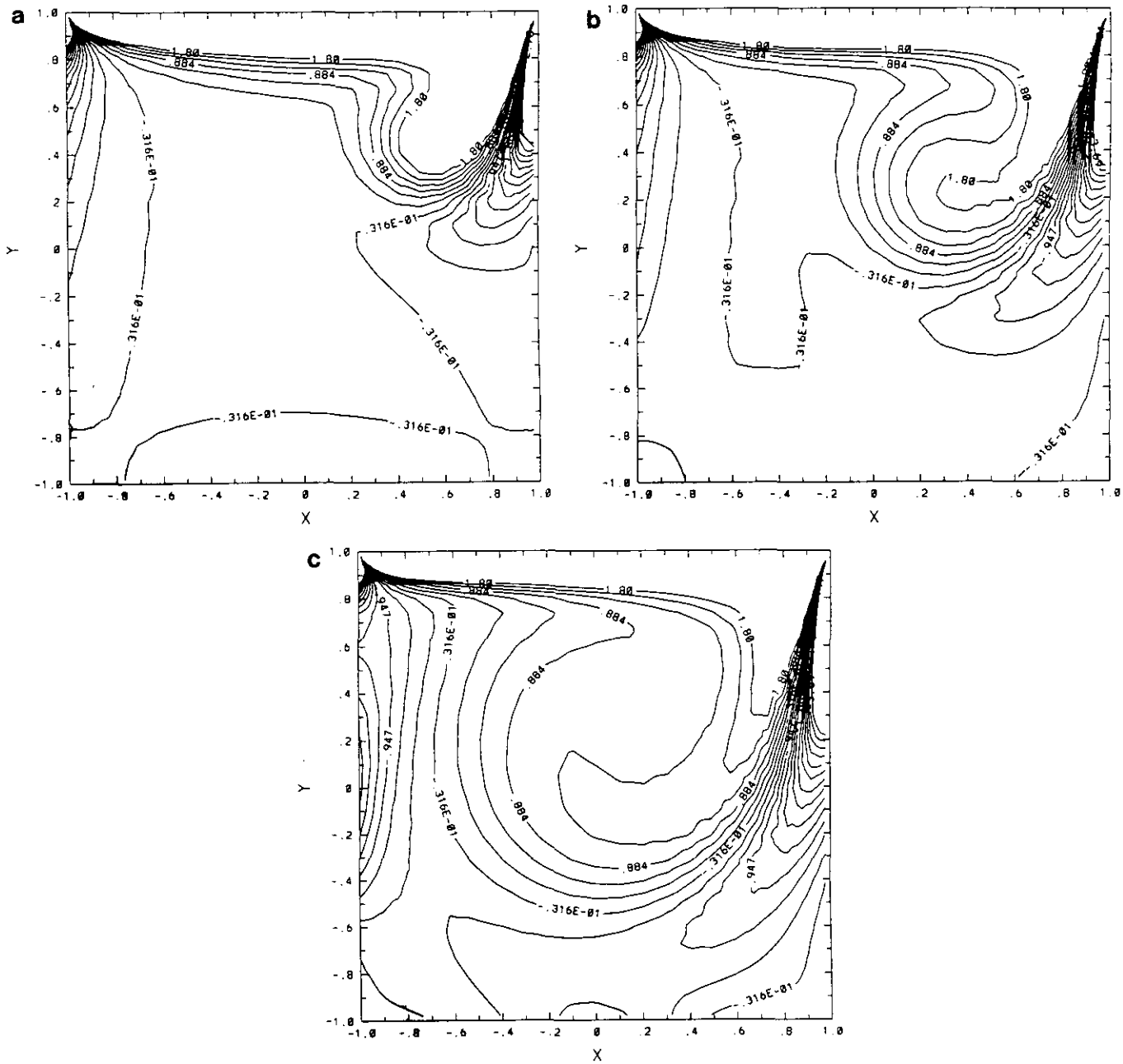

FIG. 4. Vorticity contours for Re = 400: (a) $t = 5$; (b) $t = 10$; (c) $t = 40$.

schemes. Unlike the studies of Schultz *et al.* [14] and Shen [15], where either a trick or an approximation to the boundary conditions was used, the proposed approach treats the problem in a mathematically exact and consistent manner.

Figures 2 are a series of velocity vectors depicted at four different times ($t = 0.1$, 1, 10, and 40) for Reynolds number 100. Once the lid moves, a thin layer next to it is set in motion because of the viscous actions, and within that zone the velocity changes rapidly. As the right wall is reached, the flow redirects itself in a fashion compatible to a corner, and this process is repeated at the other corners as well. The ultimate result is a complex vortex system whose structure changes continuously in time until its center finds an equilibrium position. Temporally, the flow at an early stage is very much confined in the region near the lid and the flow field is nearly symmetrical about the y-axis (see Fig. 2a). Subsequently, that region expands rapidly as illustrated in Fig. 2b at $t = 1$, where the entire cavity has already sensed the movement of the lid. If sufficient time is allowed for the

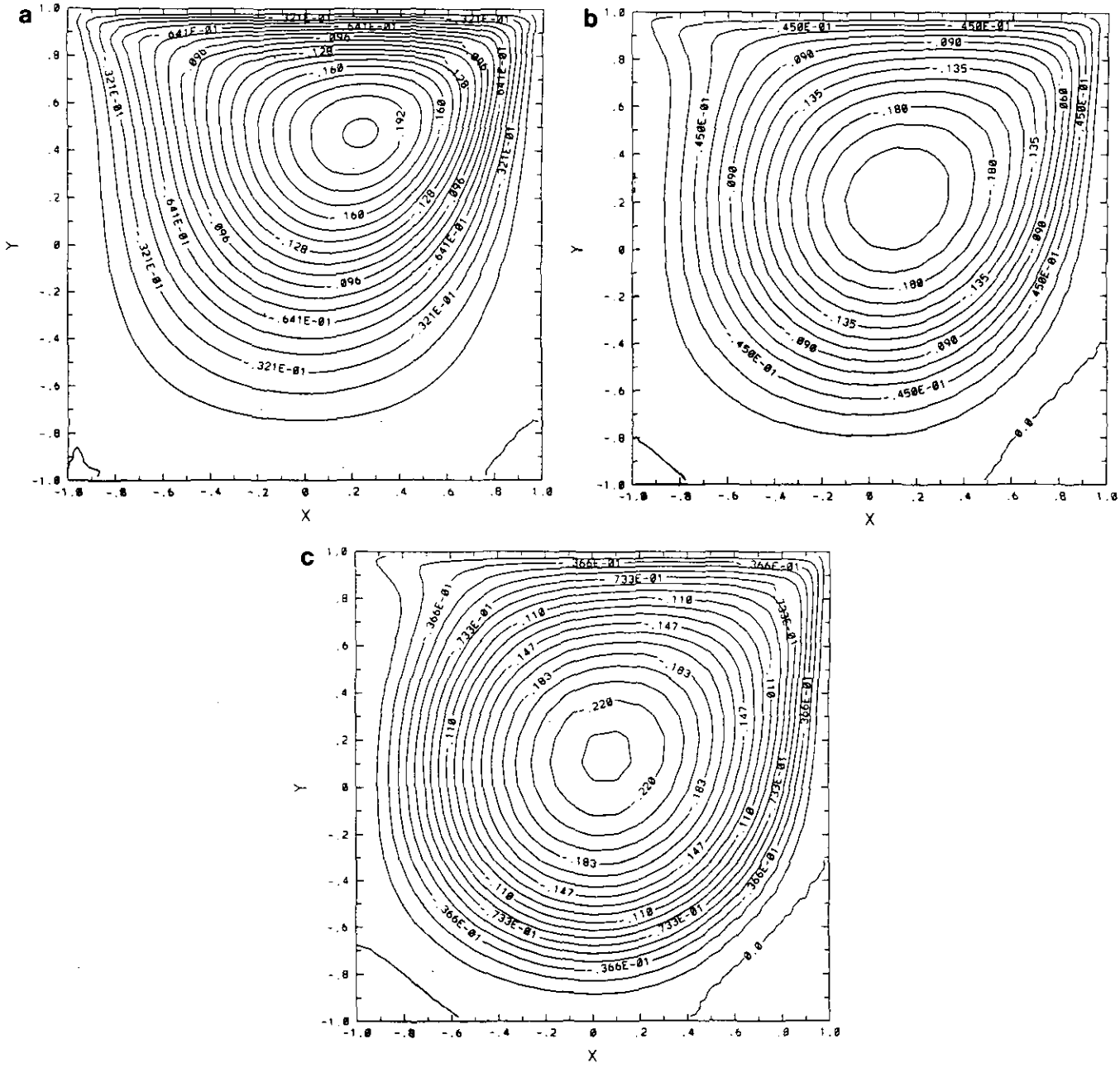

FIG. 5. Late-time stream function contours: (a) Re = 100; (b) Re = 400; (c) Re = 1000.

system to become fully developed, recirculation zones or secondary vortices form at the lower corners. Because the velocity there is so low, they are hardly distinguished from the primary vortex in the velocity vector plots, but they are visible in the contour plot of the stream function as exhibited in Fig. 5a.

To further investigate the extent to which the motion is induced to the inner region, we present the evolution of the velocity associated with $Re = 100$ along the line passing through the geometric center at various times. In Fig. 3a, the horizontal velocity along the y-axis clearly indicates the presence of a thin boundary layer which grows in time. The vertical velocity, Fig. 3b, on the other hand, shows three distinct regions consisting of boundary layer flows near the walls separated by a core within which an inflection point is seen. As an aid to our understanding of the viscous flow phenomena, the time development of the vorticity at times $t = 5$, 10, and 40 for $Re = 400$ (Fig. 4) are plotted to show the change of the vorticity structure as the vortex system develops. Also apparent in these contours are the strong singularities at the upper corners where vorticity is not unique and is, in fact, multivalued.

Figures 5 illustrate the steady-state flow patterns by stream function contours for Reynolds numbers of 100, 400, and 1000. In respective order, these results correspond to $t = 40$, 50, and 60 dimensionless time units. To assure that those are the time-invariant results, the solution is advanced continually until the relative change between the solutions of two consecutive time levels is within 0.0001 at every point in the flow domain. Attempts have been made to present our spectral results in parallel with those predicted by Ghia *et al.* [12], but the graphics are not legible for quality reproduction and are therefore not included here. In general, the basic flow structure for all three cases are comparable to those of Ghia *et al.* [12] which were obtained by a multigrid finite difference method with very fine meshes (129×129). Because of the adequacy of their solution algorithm and the spatial resolution, their solutions have been considered as benchmark results in the CFD community. In order to provide a quantitative comparison, Table I tabulates the data of the location of the main vortex center for $Re = 100$, 400, and 1000. As demonstrated in the table, the two predictive techniques agree quite well.

As an additional verification of our simulation results, comparison is carried out with respect to the horizontal velocity along the y-axis and the vertical velocity along the x-axis with the published data of Ghia *et al.* [12] in Figs. 6a and b, respectively. Again, the figures reveal exceptional agreement between the two solutions. It should be remarked that our solutions were based on a 21×21 grid for $Re = 100$, a 31×31 grid for $Re = 400$, and a 31×31 grid for $Re = 1000$, while those of Ghia and his co-workers were all based on 129×129 points. It is appropriate to point out the trend in these curves, that as the Reynolds number increases, the region where rapid change in velocity takes place becomes

TABLE I

Location of the Primary Vortex Center

	Present		Ghia *et al.* [12]	
Re	x	y	x	y
100	0.24	0.47	0.2344	0.4688
400	0.11	0.21	0.1094	0.2110
1000	0.06	0.12	0.0626	0.1250

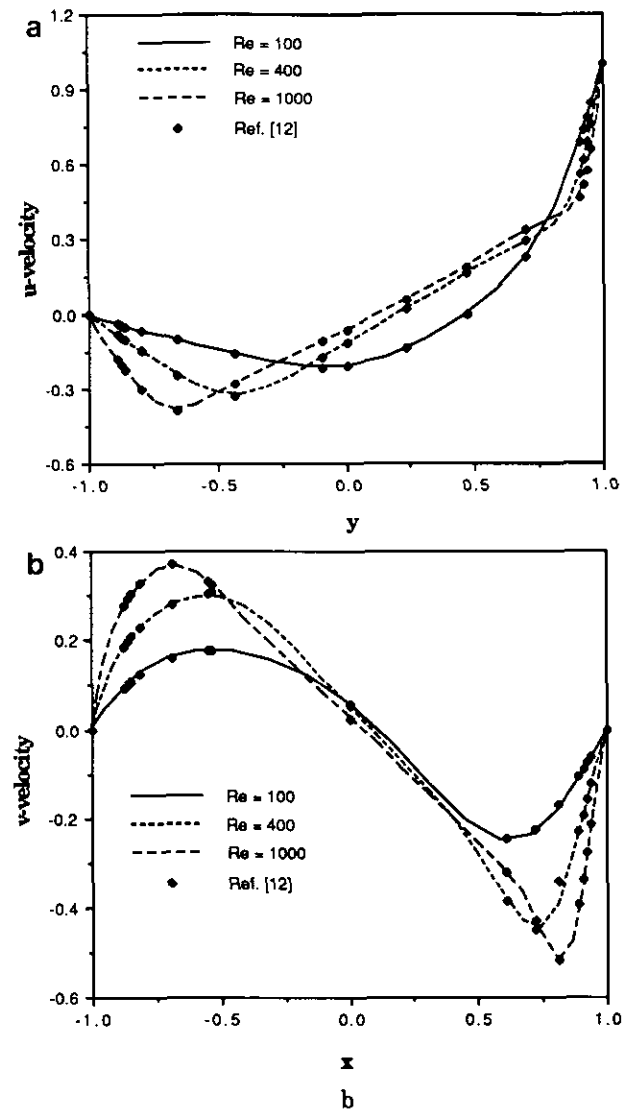

FIG. 6. Velocity comparison: (a) u-velocity along y-axis; (b) v-velocity along x-axis.

smaller and smaller. This is consistent with the boundary layer theory which had predicted the layer thickness to be on the order of the inverse of the square root of the Reynolds number.

On the basis of the above findings, it is concluded that the proposed procedure yields results comparable to those of conventional techniques with a much smaller number of unknowns because of better spatial resolution. In addition, the vorticity integral conditions can be implemented with full benefit for an accurate simulation of unsteady flows. When the conditions are employed in conjunction with a spectral discretization in space and the Adams–Bashforth/Crank–Nicolson approximation in time, an efficient non-iterative scheme for this kind of problem is obtained.

ACKNOWLEDGMENT

The authors thank Professor L. Quartapelle of the Istituto di Fisica, Politecnico Di Milano, Italy for his interest and suggestions to improve the quality of the manuscript. Thanks are also extended to Dr. Richard Johnson and Mr. Richard Martineau of EG & G Idaho, Inc. for their review. This work was performed under the auspices of the U.S. Department of Energy, Contract DE-AC07-76-ID01570, and was supported in part by the INEL Long-Term Research Initiatives Program.

REFERENCES

1. L. Quartapelle, *J. Comput. Phys.* **40**, 453 (1981).
2. L. Quartapelle and M. Napolitano, *Int. J. Numer. Methods Fluids* **4**, 109 (1984).
3. R. J. MacKinnon, G. F. Carey, and P. Murray, *Commun. Appl. Numer. Methods* **6**, 47 (1990).
4. S. C. R. Dennis and L. Quartapelle, *J. Comput. Phys.* **52**, 448 (1983).
5. A. Chaouche, A. Randriamampianina, and P. Bontoux, *Comput. Methods Appl. Mech. Eng.* **80**, 237 (1990).
6. H.-C. Ku and D. Hatziavramidis, *Comput. Fluids* **13**, 99 (1985).
7. L. Quartapelle and F. Valz-Gris, *Int. J. Numer. Methods Fluids* **1**, 129 (1981).
8. S. C. R. Dennis and L. Quartapelle, *Int. J. Numer. Methods Fluids* **9**, 871 (1989).
9. C. Canuto, M. H. Hussaini, A. Quarteroni, and T. A. Zang, *Spectral Methods in Fluid Dynamics* (Springer-Verlag, New York, 1988).
10. J. P. Boyd, *Chebyshev and Fourier Spectral Methods*, Lecture Notes in Engineering, Vol. 49 (Springer-Verlag, New York, 1989).
11. H. S. Carslaw and J. C. Jaeger, *Conduction of Heat in Solids* (Oxford University Press, New York, 1959).
12. U. Ghia, K. N. Ghia, and C. T. Shin, *J. Comput. Phys.* **48**, 387 (1982).
13. T. E. Tezduyar, J. Liou, D. K. Ganjoo, and D. Behr, *Int. J. Numer. Methods Fluids* **11**, 515 (1990).
14. W. W. Schultz, N. Y. Lee, and J. P. Boyd, *J. Sci. Comput.* **4**, 1 (1989).
15. J. Shen, *Comput. Methods Appl. Mech. Eng.* **80**, 273 (1990).